Journal of
Applied and Computational Mechanics

Shahid Chamran
University of Ahvaz

Research Paper

Effect of Inlet Air Locations on Particle Concentration using Large Eddy Simulation based on Multi Relaxation Time Lattice Boltzmann Method

Hasan Sajjadi[1,2] , Goodarz Ahmadi[3] , Amin Amiri Delouei[1,2]

[1] Department of Mechanical Engineering, University of Bojnord, Bojnord, 9453155111, Iran, Email: h.sajjadi@ub.ac.ir

[2] Center for International Scientific Studies and Collaboration, Ministry of Science, Research and Technology, Tehran, Iran

[3] Department of Mechanical and Aeronautical Engineering, Clarkson University, Potsdam, USA, Email: gahmadi@clarkson.edu

Abstract. In this work, turbulent indoor airflow was considered by Large Eddy Simulation (LES) based on Multi Relaxation Time Lattice Boltzmann Method (MRT-LBM). The Lagrangian approach was utilized to investigate the effect of inlet air location on transport and concentration of different sizes of particles (1-10 μm) in a modeled room. Simulation results showed that for the displacement ventilation system with the inlet air register on the floor, the number of 10μm particles that exit through the outlet is more than the case for the mixing ventilation system with the inlet register on the ceiling. Also, for the latter case, when the inlet air is on the ceiling, the number of suspended 10μm particles in the room is less than for the displacement ventilation system with inlet register on the floor. In addition, the results showed that the location of the inlet air register does not have a considerable effect on the small 1μm particle motion, and the numbers of the particles that remain suspended in the room are roughly the same for both ventilation systems.

Keywords: MRT-LBM, LES, Particle motion, Inlet air position, Particle concentration.

1. Introduction

Recently, understanding particle motion in the indoor environment has attracted significant attention because of their wide applications to indoor air quality (IAQ) and exposure assessment, air pollution controls, filtration and separation processes in chemical industries. Various experimental, theoretical and numerical methods were used to study the particle behavior in turbulent flows in various applications [1-8]. Sippola and Nazzarof [1] experimentally investigated the effects of particle diameter and airflow velocity on the deposition of particles in turbulent flows in ventilation ducts. They concluded that the deposition velocity to the floor of the horizontal duct is more than those to the wall, and the ceiling. Haghighifard et al. [3] used the different k-ε models to study turbulent flows and particle transport around buildings. They reported that to decline the particle deposition on a building, they should put the buildings on elevated supports, especially for 1μm particles. Ghahramani et al. [4] analyzed particle behavior in various parts of the human respiratory tract, including oropharynx, nasal cavity, and trachea by the numerical methods. They used the RANS turbulence model for considering the turbulence fluctuations effect on particle motion. They showed turbulence could enhance the sedimentation of mid-size range particles. Li et al. [5] developed a computational scheme to simulate aerosol particle motion in turbulent flows. They concluded that the deposition rate decreases significantly as the shape of the obstruction becomes more streamlined. Liu and Ahmadi [6] studied particle transport near a building model. They used a Lagrangian particle tracking computational procedure to simulate particle deposition and dispersion. Nazridoust and Ahmadi [9] analyzed the gaseous movement in various street canyons, and it is concluded that the particle deposition in street canyons decreases with the enhancement of wind speed. Dehghan and Abdolzadeh [10] studied airflow and particle transport in a 3-D dimensional room with three different locations for systems of heating. They concluded that because of the presence of the source of thermal in the modeled geometry, the particles have the tendency to exit from the room, and most of them deposited on the walls and ceiling or remain in the room. Zhong et al. [11] investigated two ventilation systems and reported that in mixing ventilation (MV), the pollutant sources location affects the concentration of injected particles and removal effectiveness, insignificantly. Also, they reported that the best efficiency for particle removal was observed for underfloor air distribution (UFAD) system. Bouilly et al. [12] studied the effect of ventilation positions on the concentration of indoor particle. They considered six various locations for the inlet and outlet and reported that for particles with $d_P < 5$μm, deposition is enhanced two times by changing the inlet/outlet configuration from the Top–Top to the Bottom–Top.

In the last three decades the LBM has been utilized and expanded extensively as a simple and efficient numerical method [13-17]. This method has been applied to simulate various flows including multi-phase flows, turbulent flows, and flows with heat

transfer [18-21]. The LBM has been utilized with different models that differ in the way they account for the collision effects. The most commonly used model is the Lattice Bhatnagar–Gross–Krook (LBGK) formulation [22, 23]. In the LBGK model, for the collision step a single relaxation time (SRT) is used. Recently, it was found that when the SRT model is applied to thermal fluids some instability was seen [24]. Therefore some investigations have been done to overcome the weaknesses of the SRT model [25-27]. Ginzburg [25] reported a suitable model for both heat and fluid flow which is used two-relaxation-time (TRT) for the collision step instead of SRT model. Chikatamarla et al. [26] presented a new model, the entropic Lattice Boltzmann Model (ELBM), and reported that this new model guarantees stability and thermodynamic consistency. Luo et al. [27] performed a comparative study and evaluated various models for the collision step for incompressible flows which named (TRT), (SRT), (ELBM), and multiple-relaxation-time (MRT). They concluded that the TRT and MRT models are better than the ELBE and SRT models in terms of computational efficiency, accuracy, and stability. Recently Sajjadi et al. [28-30] used the MRT-LBM method to simulate various flow fields in a different geometry. They showed that the MRT-LBM method can predict the result more accurately in comparison with the earlier works.

The large eddy simulation (LES) solves the large eddies in turbulent flows and models only the fluctuations that are smaller than the grid size. The LES approach typically provides more accurate results for mean turbulent airflow properties compares to the RANS models and also provides the instantaneous turbulence fluctuation velocities that are larger than the grid size. Due to these advantages, the use of the LES model for simulating indoor airflows has markedly increased in the last decade [31-33]. Zhou et al. [34] used the LBM-LES to solve the turbulent flow around a circular cylinder. They reported that the results obtained with the LBM-LES model agree well with both experimental data and earlier numerical results. Merlier et al. [35] used an innovative Lattice Boltzmann (LB) - LES approach to solve pollutant dispersion in urban environments for neutral and stratified conditions. They compared the predicted pollutant concentrations with the wind tunnel measurements and reported good agreements. Sajjadi et al. [36 and 37] investigated the particle motion in a modeled room using the LBM and different turbulence models, (LES), Reynolds Averaged Navier-Stokes (RANS) model, and HYBRID method. They reported that these models can capture the features of particle dispersion and deposition reasonably well. The LBM-LES model is, however, the most accurate for prediction of particle deposition rate and concentration in the indoor environment, which followed by the HYBRID and the RANS methods. Immersed boundary – lattice Boltzmann method is also another technique that is used for simulation of stationary [38 and 39] and moving [40 and 41] boundaries.

In this study, the MRT-LBM-LES method was used, and the particle transport, dispersion, and deposition in a modeled room were predicted for different ventilation systems. Particular attention was given to the effect of inlet air register on particle deposition and variation of concentration in the room. Also, different particle sizes were investigated, and the effect of particle size on particle transport and deposition was discussed.

2. Room Geometry

To reduce the simulation time and cost, a scaled room model, which is the one-tenth scale of a typical office is investigated in this work. Schematics of the room with displacement and mixing ventilation systems are shown in Fig. 1. In the present study, incompressible assumption is used for the fluid and the airflow is the turbulent regime, with the Reynolds number based on the inlet velocity of Re=1500. In addition, to investigate the effect of inlet air location on airflow and particle motion for displacement and mixing ventilation systems, the cases that the inlet register is on the flow and on the ceiling are considered. The outlet air register bother cases are on the ceiling. The inlet and outlet are squares with the dimensions of 0.101 m×0.101 m.

3. Multi Relaxation Time Lattice Boltzmann Method (MRT-LBM)

MRT-LBM with D3Q19 lattice, as shown in Fig. 2, is used in this study to solve the 3-D turbulent flows under various conditions. The following equation is used to calculate the distribution function for incompressible flows [37]:

$$f_i(x + c_i \Delta t, t + \Delta t) = f_i(x,t) - M_{ij}^{-1}.S_{jk}.[R_k(x,t) - R_k^{eq}(x,t)]$$

(1)

In eq. (1) f_i is the velocity distribution function and is used to calculate the density and macroscopic velocity. Δt is the lattice time step and was set to unity, c_i is the discrete fluid particle velocity vectors are shown in Fig. 2.

$$c_i = \begin{cases} (0,0) & i = 0 \\ c(\pm 1,0,0), c(0,\pm 1,0), c(0,0,\pm 1) & i = 1-6 \\ c(\pm 1,\pm 1,0), c(\pm 1,0,\pm 1), c(0,\pm 1,\pm 1) & i = 7-18 \end{cases}$$
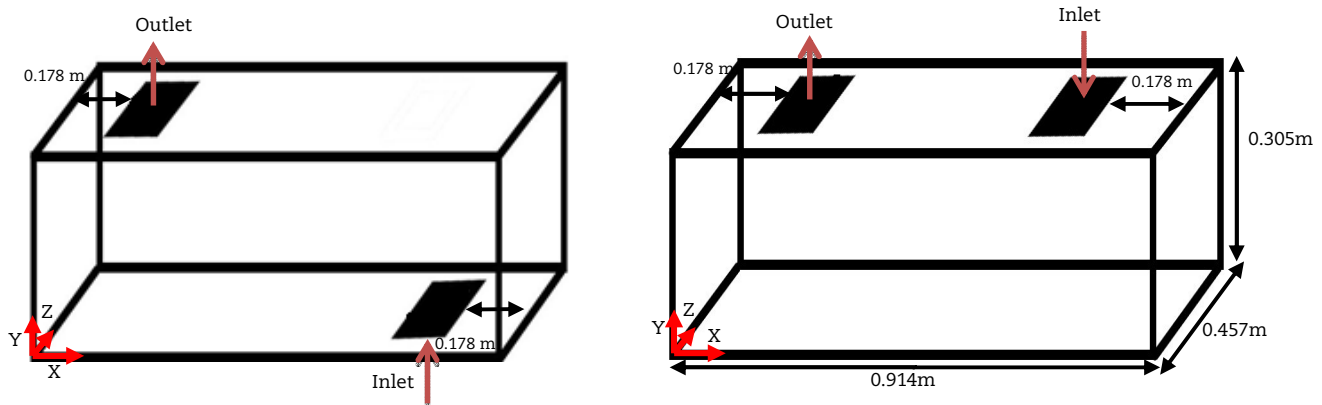
(2)

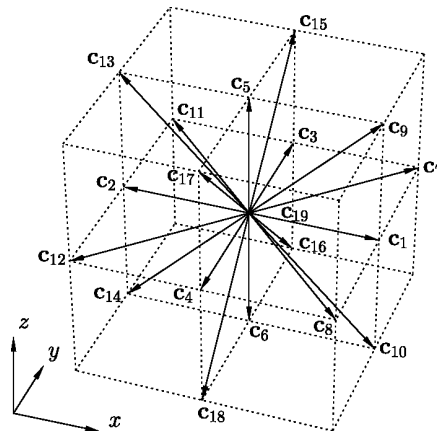**Fig. 1.** The studied room configurations with displacement and mixing ventilation systems

Fig. 2. Discrete velocity vectors for D3Q19

M_{ij} is the transformation matrix and is defined as,

$$
M = \begin{pmatrix}
1 & 1 & 1 & 1 & 1 & 1 & 1 & 1 & 1 & 1 & 1 & 1 & 1 & 1 & 1 & 1 & 1 & 1 & 1 \\
-30 & -11 & -11 & -11 & -11 & -11 & -11 & 8 & 8 & 8 & 8 & 8 & 8 & 8 & 8 & 8 & 8 & 8 & 8 \\
12 & -4 & -4 & -4 & -4 & -4 & -4 & 1 & 1 & 1 & 1 & 1 & 1 & 1 & 1 & 1 & 1 & 1 & 1 \\
0 & 1 & -1 & 0 & 0 & 0 & 0 & 1 & -1 & 1 & -1 & 1 & -1 & 1 & -1 & 0 & 0 & 0 & 0 \\
0 & -4 & 4 & 0 & 0 & 0 & 0 & 1 & -1 & 1 & -1 & 1 & -1 & 1 & -1 & 0 & 0 & 0 & 0 \\
0 & 0 & 0 & 1 & -1 & 0 & 0 & 1 & 1 & -1 & -1 & 0 & 0 & 0 & 0 & 1 & -1 & 1 & -1 \\
0 & 0 & 0 & -4 & 4 & 0 & 0 & 1 & 1 & -1 & -1 & 0 & 0 & 0 & 0 & 1 & -1 & 1 & -1 \\
0 & 0 & 0 & 0 & 0 & 1 & -1 & 0 & 0 & 0 & 0 & 1 & 1 & -1 & -1 & 1 & 1 & -1 & -1 \\
0 & 0 & 0 & 0 & 0 & -4 & 4 & 0 & 0 & 0 & 0 & 1 & 1 & -1 & -1 & 1 & 1 & -1 & -1 \\
0 & 2 & 2 & -1 & -1 & -1 & -1 & 1 & 1 & 1 & 1 & 1 & 1 & 1 & 1 & -2 & -2 & -2 & -2 \\
0 & -4 & -4 & 2 & 2 & 2 & 2 & 1 & 1 & 1 & 1 & 1 & 1 & 1 & 1 & -2 & -2 & -2 & -2 \\
0 & 0 & 0 & 1 & 1 & -1 & -1 & 1 & 1 & 1 & 1 & -1 & -1 & -1 & -1 & 0 & 0 & 0 & 0 \\
0 & 0 & 0 & -2 & -2 & 2 & 2 & 1 & 1 & 1 & 1 & -1 & -1 & -1 & -1 & 0 & 0 & 0 & 0 \\
0 & 0 & 0 & 0 & 0 & 0 & 0 & 1 & -1 & -1 & 1 & 0 & 0 & 0 & 0 & 0 & 0 & 0 & 0 \\
0 & 0 & 0 & 0 & 0 & 0 & 0 & 0 & 0 & 0 & 0 & 0 & 0 & 0 & 0 & 1 & -1 & -1 & 1 \\
0 & 0 & 0 & 0 & 0 & 0 & 0 & 0 & 0 & 0 & 0 & 1 & -1 & -1 & 1 & 0 & 0 & 0 & 0 \\
0 & 0 & 0 & 0 & 0 & 0 & 0 & 1 & -1 & 1 & -1 & -1 & 1 & -1 & 1 & 0 & 0 & 0 & 0 \\
0 & 0 & 0 & 0 & 0 & 0 & 0 & -1 & -1 & 1 & 1 & 0 & 0 & 0 & 0 & 1 & -1 & 1 & -1 \\
0 & 0 & 0 & 0 & 0 & 0 & 0 & 0 & 0 & 0 & 0 & 1 & 1 & -1 & -1 & -1 & -1 & 1 & 1
\end{pmatrix}
\tag{3}
$$

In eq. (1) S_{jk} is the diagonal matrix of relaxation rates. Where $S_{jk} = diag(s_0, s_1, ..., s_{18})$ and the components of S_{jk} for the present work are evaluated as [37],

$$
\begin{aligned}
&S_0 = S_3 = S_5 = S_7 = 0. \\
&S_1 = 1.19 \\
&S_9 = S_{11} = S_{13} = S_{14} = S_{15} = \frac{1}{(3\nu + 0.5)} \\
&S_2 = S_{10} = S_{12} = 1.4 \\
&S_4 = S_6 = S_8 = 1.2 \\
&S_{16} = S_{17} = S_{18} = 1.98
\end{aligned}
\tag{4}
$$

where ν is the kinematic viscosity and calculate as $\nu = \nu_0 + \nu_t$. In this work, ν_0 is set as:

$$
\nu_0 = \frac{U_{in} \times L}{Re}
\tag{5}
$$

where U_{in} is the inlet velocity, L is the characteristic length, which is the length of the inlet gate, and Re is the Reynolds number of the flow. To evaluate the turbulent viscosity, ν_t, the standard Smagorinsky model is used as:

$$
\nu_t = (C_S \Delta)^2 |G|
\tag{6}
$$

where C_s is the Smagorinsky constant and is set to 0.16. Δ is the mean grid size and obtained as $\Delta = (\Delta x \Delta y \Delta z)^{1/3}$. In eq. (6) $|G|$ is the mean of strain rate tensor and calculated by $|G| = \sqrt{2G_{\alpha\beta}G_{\alpha\beta}} = \sqrt{2[G_{xx}^2 + G_{yy}^2 + G_{zz}^2 + 2(G_{xy}^2 + G_{yz}^2 + G_{xz}^2)]}$ where $G_{\alpha\beta}$ are given as [37]:

$$G_{xx} = -\frac{1}{38\rho}[s_1 h_1^{neq} + 19 s_9 h_9^{neq}] \tag{7}$$

$$G_{yy} = -\frac{1}{76\rho}[2 s_1 h_1^{neq} - 19(s_9 h_9^{neq} - 3 s_{11} h_{11}^{neq})] \tag{8}$$

$$G_{zz} = -\frac{1}{76\rho}[2 s_1 h_1^{neq} - 19(s_9 h_9^{neq} + 3 s_{11} h_{11}^{neq})] \tag{9}$$

$$G_{xy} = -\frac{3}{2\rho} s_{13} h_{13}^{neq} \tag{10}$$

$$G_{yz} = -\frac{3}{2\rho} s_{14} h_{14}^{neq} \tag{11}$$

$$G_{xz} = -\frac{3}{2\rho} s_{15} h_{15}^{neq} \tag{12}$$

where $h_\alpha^{neq} = R_\alpha - R_\alpha^{eq}$. R in eq. (1) is defined as $R = MF$, where F is the matrix of velocity distributions function (f). After calculating the velocity distributions function using eq. (1) the macroscopic velocity and density are calculated using,

$$\rho(x,t) = \sum_i f_i(x,t), \ \ \rho u(x,t) = \sum_i f_i(x,t) c_i, \tag{13}$$

4. Particle Equation

Small particles motion equation is given by [42]:

$$\frac{du_i^p}{dt} = \frac{1}{\tau_p}\frac{C_D \, \mathrm{Re}_p}{24}(u_i - u_i^p) + (1 - \frac{1}{s})g_i + n_i(t) \tag{14}$$

Here the lift force has been neglected. In eq. (14) u_i^p is the particle velocity, and u_i is the fluid velocity at the particle location. τ_p is defined as the particle relaxation time $\tau_p = Sd^2 C_c / 18\nu$. Here S is the ratio of particle density to fluid density, d is the particle diameter, ν is the kinematic viscosity of the fluid, and C_c is the Cunningham slip correction defined as,

$$C_c = 1 + \frac{2\lambda}{d}(1.257 + 0.4 e^{\frac{-1.1d}{\lambda}}) \tag{15}$$

In eq. (15), λ is the molecular mean free path of the gas and equal to 7×10^{-8}m. C_D in the first term on the right-hand side of eq. (14) is the drag coefficient and is calculated based on the particle Reynolds number (Re_p) as,

$$C_D = \frac{24}{\mathrm{Re}_p}(1 + 0.15 \mathrm{Re}_p^{0.687}) \qquad \mathrm{Re}_p < 400 \tag{16}$$

where $\mathrm{Re}_p = d|u_i - u_i^p|/\nu$. The second term in the right-hand side of eq. (14) is the gravity/buoyancy force and g_i is the acceleration of gravity, which is in the z-direction. The last term in eq. (14) is the Brownian force which is calculated using a Gaussian white noise random process as [43],

$$n_i(t) = \zeta_i \sqrt{\frac{\pi S_1}{\Delta t}} \tag{17}$$

where $S_1 = 216\nu k_b T / \pi^2 \rho d^5 S^2 C_c$, k_b is the Boltzmann constant and ζ is a zero mean, unit variance independent Gaussian random number.

To calculate the average particle concentration in the room, a combined method of Hardalupas and Taylor [44] and Zhu et al. [45] was used. Where, concentration is calculated with respect to the ratio of the residence time to the total time as the following equation [46],

$$C = \frac{\sum_{i=1}^{n} t_i}{VT} \tag{18}$$

where V is the measurement volume and n is the number of the particles that pass through the V, and t_i is the particle residence time in the measurement volume during the sampling time T. Also, it should be pointed out that the concentrations are evaluated on a predefined mesh that is not the same as the computation mesh. In this work, the average concentration at the inlet was used to normalize the computed concentrations in the midplane and the normalized concentration is,

$$C^* = \frac{\sum_{i=1}^{n} t_i / V}{(N/A_{in} v_{in})} \tag{19}$$

where N is the number of injected particles with the velocity of v_{in} at the inlet area of A_{in}.

5. Results and Discussions

5.1 Code validation

To check the accuracy of the present computational model, the present simulation for flow field and particle transport is validated with the earlier experimental data and LES simulation of Posner et al. [47], Tian et al. [48] and Sajjadi et al. [37] that used a similar room model with inlet register on the ceiling. Here an inlet airflow velocity of 0.1 LL/LT. Figure 3 compares the present time-averaged inlet jet centerline axial velocity with the results of [33, 47 and 48]. It is seen that the present simulations for the airflow field are in good agreement with the earlier experimental and LES results with an error of less than 3%.

In the study of Tian et al. [48] and Sajjadi et al. [37], when the flow reaches the quasi-steady state, 86400 particles with the same velocity as the inlet air are injected into the room from the inlet vent for the time duration of 30s (every 0.05s, 144 particles are injected) and then the particle injection is stopped. Particle density was 800 kg/m3. Comparisons of the number of suspended 1μm particles with the earlier works are shown in Fig. 4. It is seen that the present simulation is in agreement with the earlier LES results, with the maximum error of about 15%. It should be pointed out that the study of [37, 47 and 48] had a partition in the middle of the room (Figure 5) that could be the cause for the differences seen here.
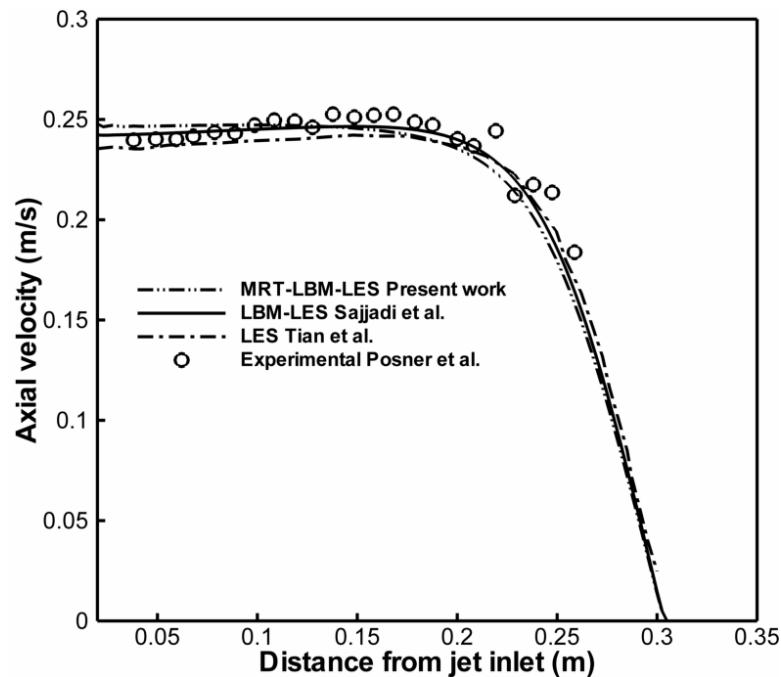
Fig. 3. Comparison of the time-averaged vertical velocity along the inlet jet axis with previous results of [37, 47, 48].
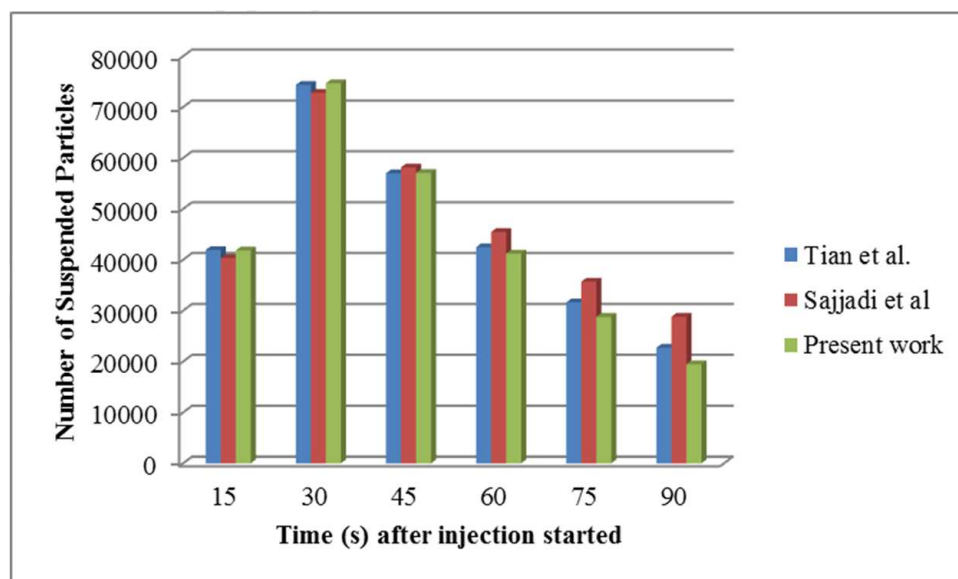

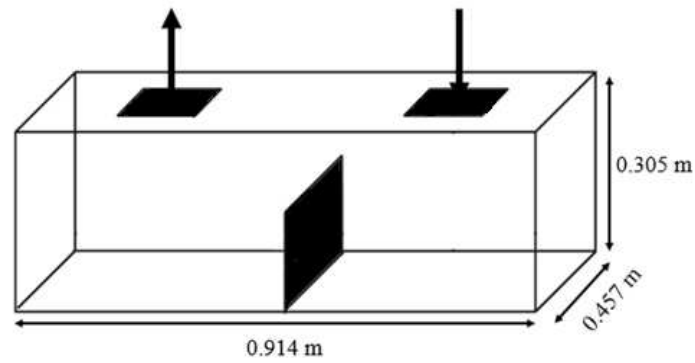**Fig. 4.** Comparison of the number of suspended 1 μm particles in the room with the previous works [37, 47].

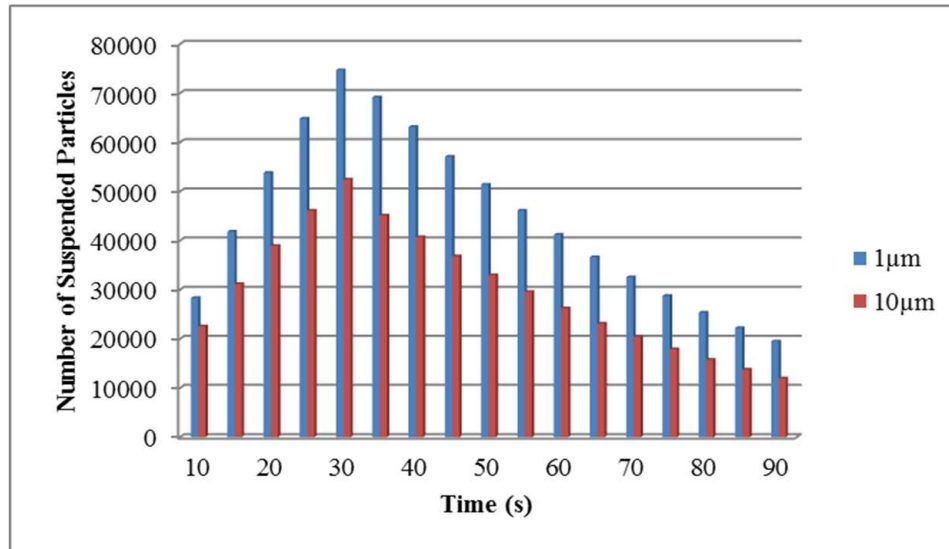**Fig. 5.** Earlier studied room geometry with partition [37, 47, 48].

Fig. 6. Number of suspended particles in the room with inlet air location on the ceiling
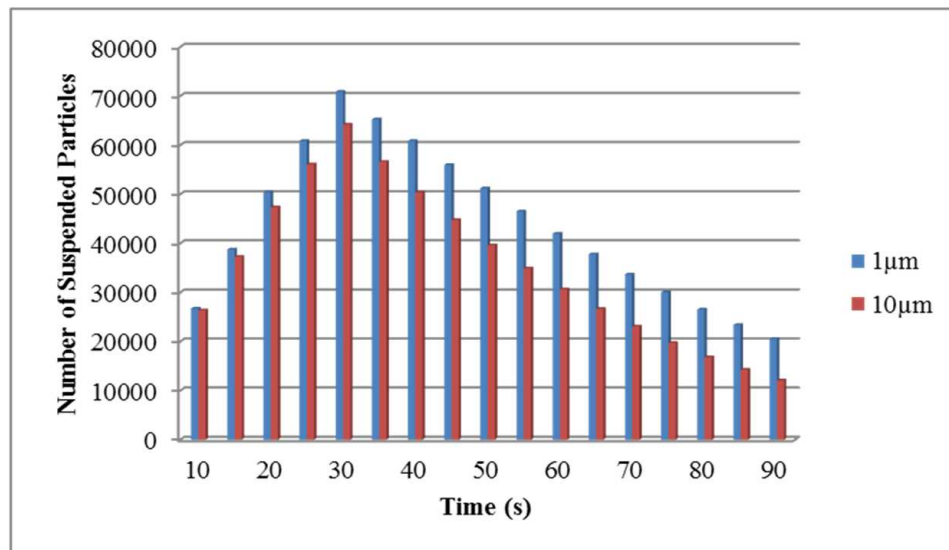

Fig. 7. The time variation of the number of suspended particles in the room with inlet air location on the floor.

5.2 Effect of particle sizes

For particle simulation, similar to the earlier work after the flow reaches a quasi-steady state, every 0.05 seconds 144 particles injected with the inlet velocity from the inlet position for 30 seconds, so 86400 particles were injected, and the density of particles was 800 kg/m^3.To investigate the effect of size on particle dispersion in the room, a large number of suspended 1 and 10 μm particles in the room for both ventilation systems (inlet air location on the ceiling and floor) are evaluated, and the results are shown in Figs. 6 and 7. It is seen that the number of suspended 1 μm particles for both configurations are more than 10 μm particles. Also, for the inlet vent on the ceiling, the number of suspended 10 μm particles is less than the case when the inlet register is on the floor. This because most of the 10 μm particles deposited on the floor for ceiling inlet register due to the same direction of jet momentum and gravity.

### 5.3 Effect of inlet air location

Time variations of 1 and 10 µm particle concentrations for different locations of the inlet air register are shown in Figs. 8, 9, 10, and 11. It is seen that the particle concentration on the left side, where the outlet is located, increases with time for both geometries and particle sizes. Most of the 1µm particles followed the airflow field and moved to the left side of the room. Due to gravity, however, the 10 µm particles remain partly suspended on the right side of the room, where the particles are injected, or deposit on the walls; therefore, the concentration on the left side for 1µm particles is more than 10µm.
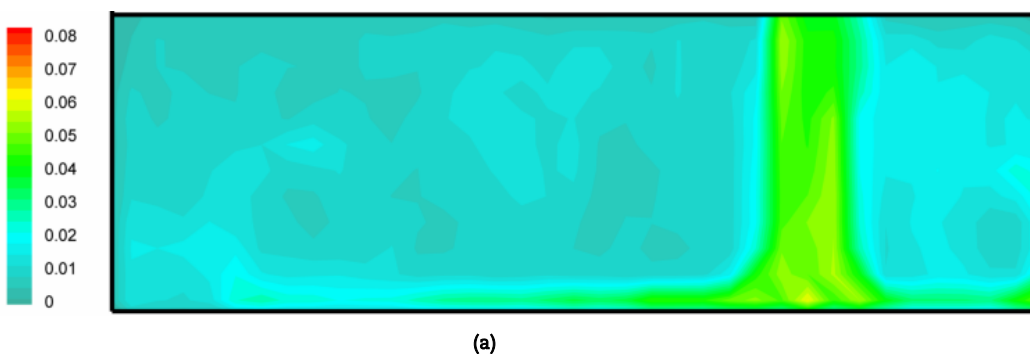
When the inlet air located on the ceiling, the particle concentration near the floor is more than the other walls of the room because the directions of the inlet airflow and gravity force are the same (Figures 8 and 10). In contrast to the ceiling position, the maximum particle concentration when the inlet air is located on the floor is on the ceiling because the gravity force for 1 µm particles is low and particles follow the inlet flow direction toward the ceiling (Figure 9), but for 10µm particles concentration near the ceiling is less than 1 µm because the gravity force affects the big particles more and 10µm particles move to the bottom wall (Figure 11).

(a)

(b)

(c)

(d)
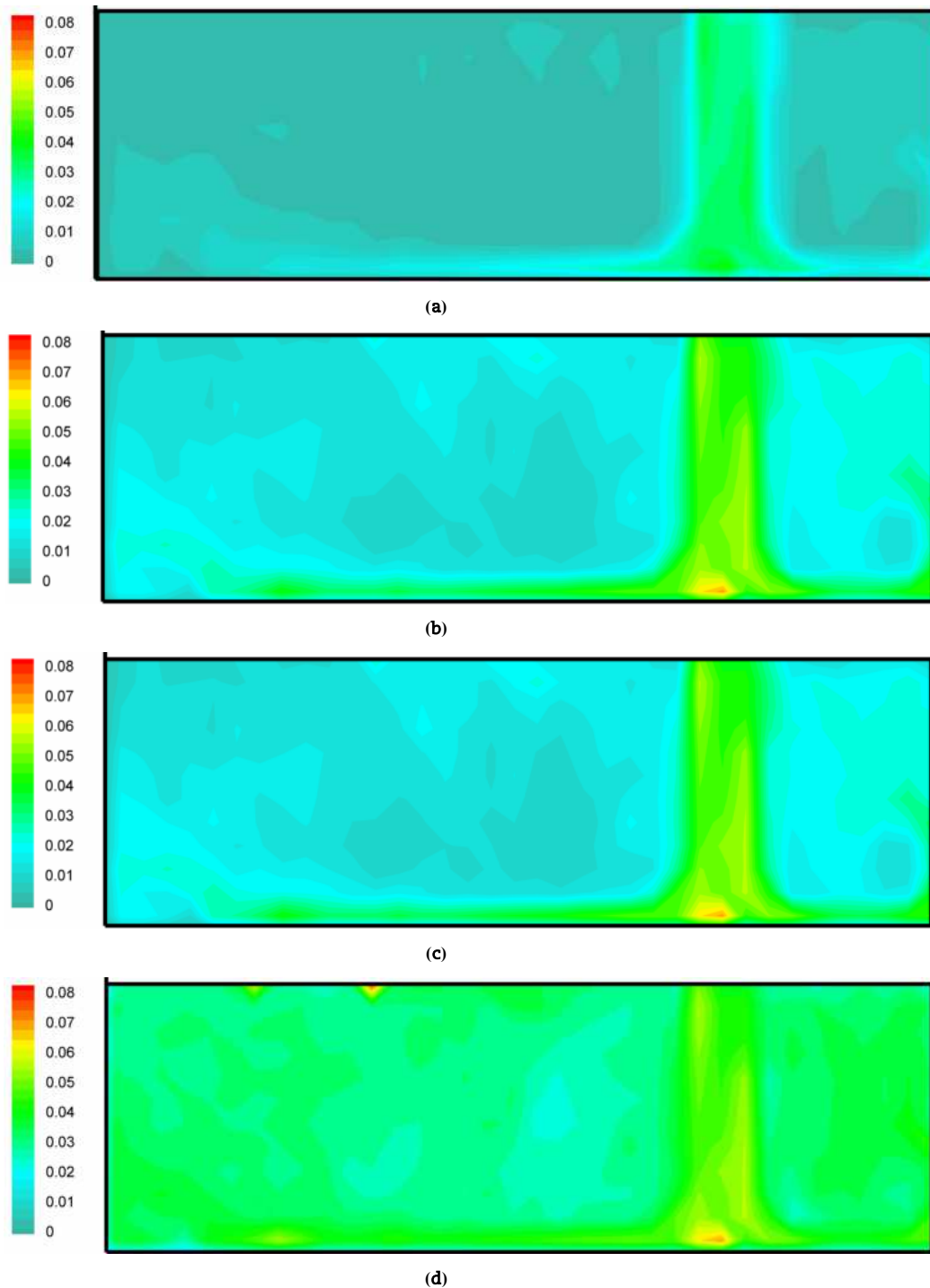
Fig. 8. Particle concentration contours at the mid-plane of the room at different times after injection of 1 µm particles for inlet air vent on the ceiling. a) 20s. b) 40s. c) 60s. d) 80s.
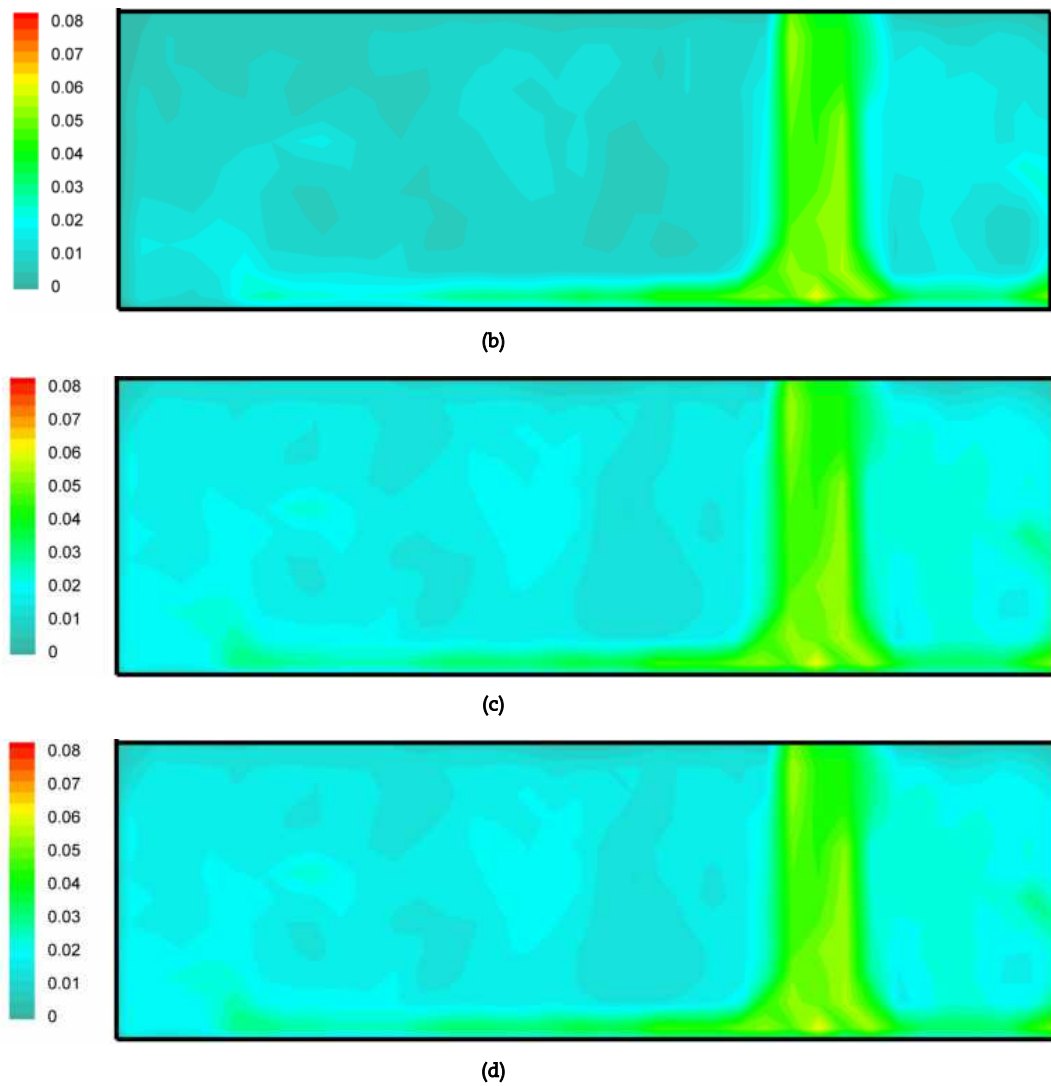
(a)

(b)

(c)

(d)
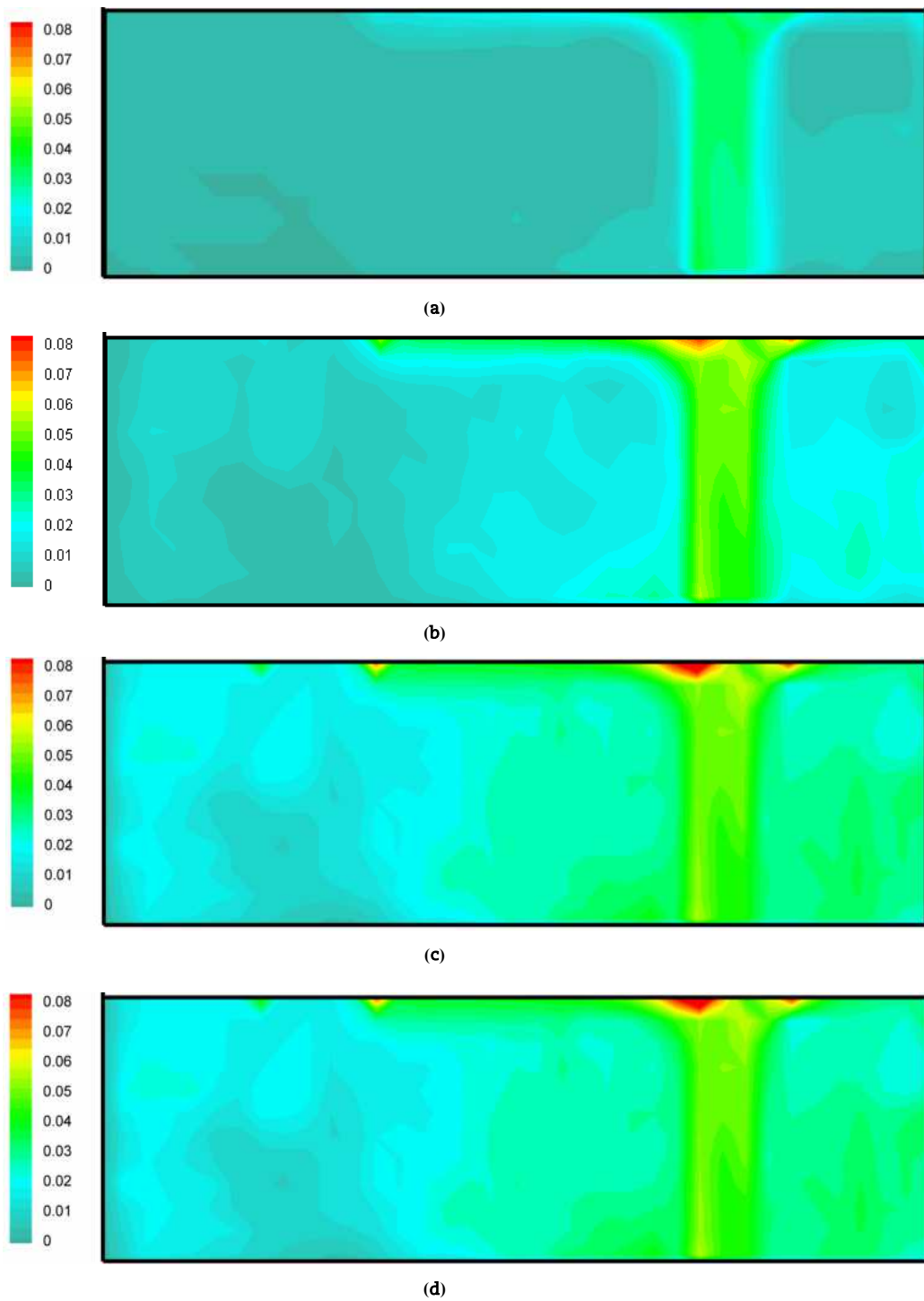
Fig. 9. Particle concentration contours at the mid-plane of the room at different times after injection of 1 μm particles for inlet air vent on the Floor. a) 20s. b) 40s. c) 60s. d) 80s.
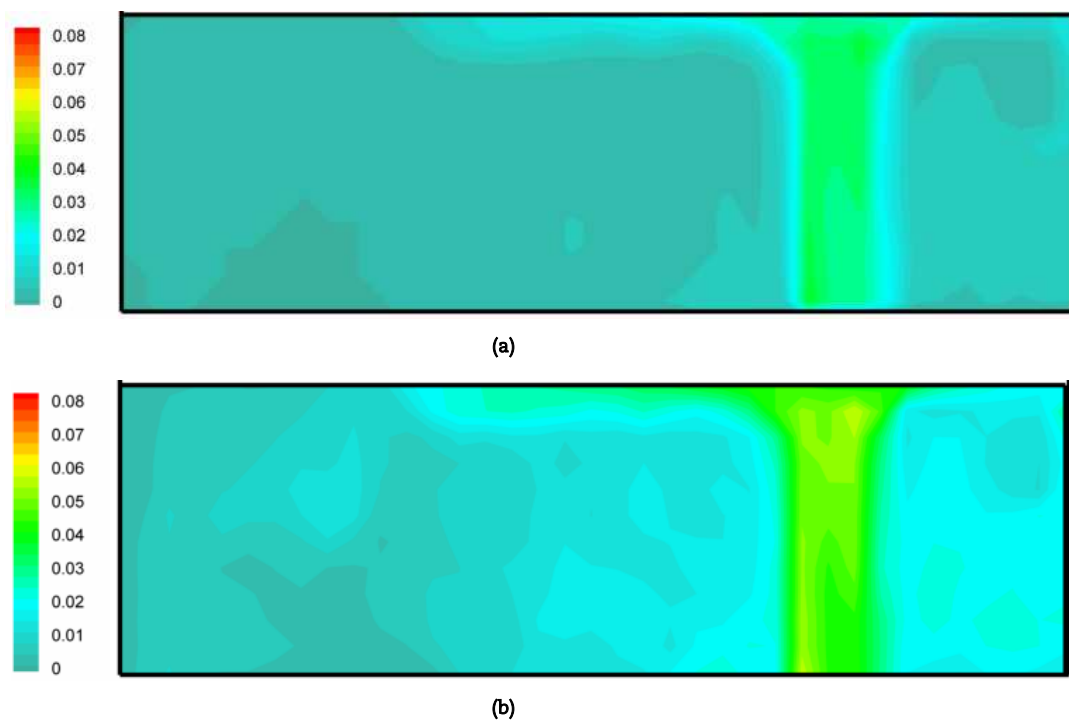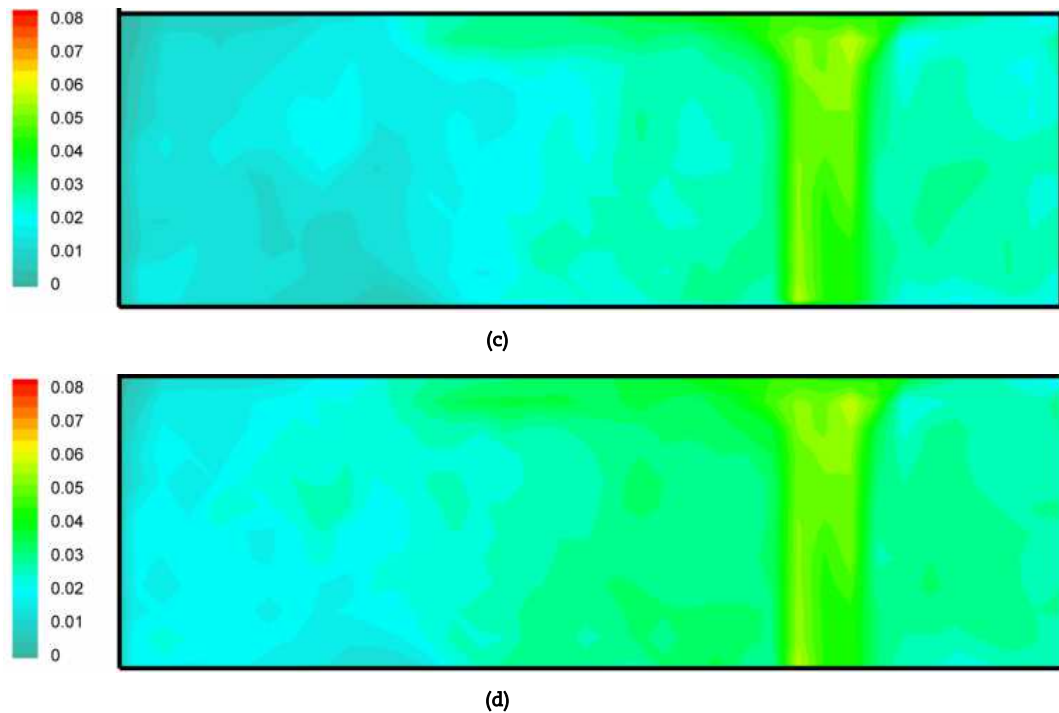

(a)

Fig. 10. Particle concentration contours at the mid-plane of the room at different times after injection of 10 μm particles for inlet air vent on the ceiling. a) 20s. b) 40s. c) 60s. d) 80s

(b)

(c)

(d)

Fig. 10. Particle concentration contours at the mid-plane of the room at different times after injection of 10 μm particles for inlet air vent on the ceiling. a) 20s. b) 40s. c) 60s. d) 80s

(a)

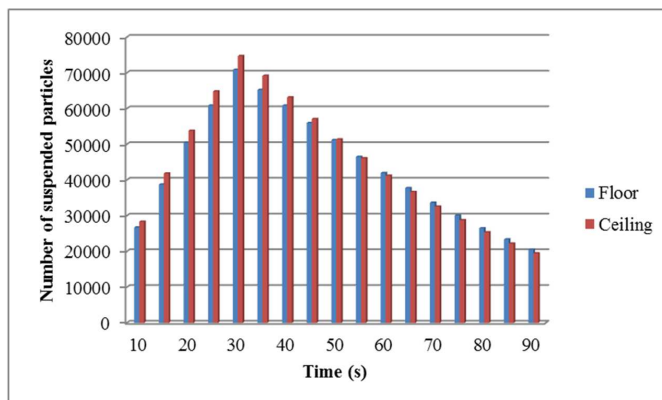(b)

Fig. 11. Particle concentration contours at the mid-plane of the room at different times after injection of 10 μm particles for inlet air vent on the ceiling. a) 20s. b) 40s. c) 60s. d) 80s

(c)

(d)
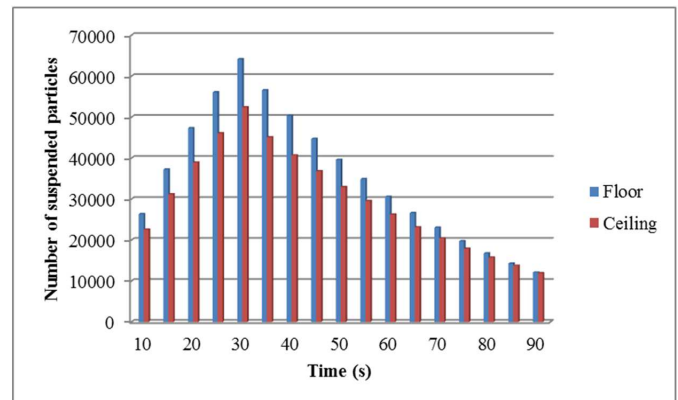
Fig. 11. Particle concentration contours at the mid-plane of the room at different times after injection of 10 μm particles for inlet air vent on the ceiling. a) 20s. b) 40s. c) 60s. d) 80s

Fig. 12. Time variation of the number of suspended 1 μm particles in the room for various inlet air locations.

Fig. 13. Time variations of the number of suspended 10 μm particles in the room for various inlet air locations.

The numbers of suspended 1 and 10 μm particles by time in the room for various locations of inlet air register are shown in Figs. 12 and 13. It is seen that for the 1 μm particles when the inlet air vent is on the ceiling, the number of suspended particles is more than that on the floor and the maximum difference is 6% (Figure 12). But for the 10 μm particles number of suspended particle for floor location is more than ceiling because most of the 10 μm particles deposited on the floor when the location is fixed on the ceiling due to gravity force and maximum differences are 25% (Figure 13).

6. Conclusions

The MRT-LBM-LES was used for simulation of turbulent airflow and particle transport in a scaled room with two different locations for inlet air register. Two sizes of particles (1 and 10 μm) were considered, and particle concentration and the number of suspended particles in the modeled room for various locations of the inlet vent were reported. The results show that the particle concentration near the floor is more than those near the room walls when the inlet air is located on the ceiling. The concentration near the ceiling is more than the other room walls when the inlet air register is located on the floor. Also, when the inlet air vent is on the ceiling, the number of suspended 1 μm particles is more than that on the floor, and the maximum difference is 6%. In addition, when the inlet air register is on the ceiling, the number of suspended 10 μm particles in the room is less than the case when the inlet vent is on the floor, and the maximum difference is 25%.

Authors Contributions

Acknowledgment

Conflict of Interest

The authors declared no potential conflicts of interest with respect to the research, authorship, and publication of this article.

Nomenclature

f_i	Velocity distribution	U_{in}	Inlet velocity
ν	Kinematic viscosity	Re	Reynolds number
ν_0	Initial Kinematic viscosity	u	Velocity
ν_t	Turbulent Kinematic viscosity	ρ	Density

References

[1] Sippola, M. R., Nazaroff, W. W., Experiments Measuring Particle Deposition from Fully Developed Turbulent Flow in Ventilation Ducts, *Aerosol Science and Technology*, 38, 2004, 914-925.

[2] Islam, M. S., Saha, S. C., Gemci, T., Yang, I. A., Sauret, E., Gu, Y. T., Polydisperse Microparticle Transport and Deposition to the Terminal Bronchioles in a Heterogeneous Vasculature Tree, *Scientific Reports*, 8, 2018, 16387.

[3] Haghighifard, H. R., Tavakol, M. M., Ahmadi, G., Numerical study of fluid flow and particle dispersion and deposition around two inline buildings, *Journal of Wind Engineering & Industrial Aerodynamics*, 179, 2018, 385–406.

[4] Ghahramani, E., Abouali, O., Emdad, H., Ahmadi, G. , Numerical analysis of stochastic dispersion of micro-particles in turbulent flows in a realistic model of human nasal/upper airway, *Journal of Aerosol Science*, 67, 2014, 188–206.

[5] Li, A., Ahmadi, G. , Bayer, R. G., Gaynes, M. A., Aerosol particle deposition in an obstructed turbulent duct flow, *Journal of Aerosol Science*, 25, 1994, 91-112.

[6] Liu, C., Ahmadi, G., Transport and deposition of particles near a building model, *Building and Environment*, 41, 2006, 828–836.

[7] Ching, J., Kajino, M., Aerosol mixing state matters for particles deposition in human respiratory system, *Scientific Reports*, 8, 2018, 8864.

[8] HOUNAM, R. F., BLACK, A., WALSH, M., Deposition of Aerosol Particles in the Nasopharyngeal Region of the Human Respiratory Tract, *Nature*, 221, 1969, 1254–1255.

[9] Nazridoust, K., Ahmadi, G., Airflow and pollutant transport in street canyons, *Journal of Wind Engineering and Industrial Aerodynamics*, 94, 2006, 491–522.

[10] Dehghan, M.H., Abdolzadeh, M., Comparison study on air flow and particle dispersion in a typical room with floor, skirt boarding, and radiator heating systems, *Building and Environment,* 133, 2018, 161-177.

[11] Zhong, K., Yang, X., Kang, Y., Effects of ventilation strategies and source locations on indoor particle deposition, *Building and Environment,* 45, 2010, 655–662.

[12] Bouilly, J., Limam, K., Beghein, C., Allard, F., Effect of ventilation strategies on particle decay rates indoors: an experimental and modelling study, *Atmospheric Environment*, 39, 2005, 4885–92.

[13] Kefayati, GH.R., Tang, H., MHD thermosolutal natural convection and entropy generation of Carreau fluid in a heated enclosure with two inner circular cold cylinders, using LBM, *International Journal of Heat and Mass Transfer Volume*, 126, 2018, 508-530.

[14] Kefayati, GH.R., Magnetic field effect on heat and mass transfer of mixed convection of shear-thinning fluids in a lid-driven enclosure with non-uniform boundary conditions, *Journal of the Taiwan Institute of Chemical Engineers*, 51, 2015, 20-33.

[15] Sajjadi, H., Kefayati, GH.R., Lattice Boltzmann simulation of turbulent natural convection in tall enclosures, *Thermal science*, 19, 2015, 155-166.

[16] Sajjadi, H., Kefayati, GH.R., MHD Turbulent and Laminar Natural Convection in a Square Cavity utilizing Lattice Boltzmann Method, *Heat Transfer Asian Research*, 45, 2016, 795-814.

[17] Jalali, A., Amiri Delouei, A., Khorashadizadeh, M., Golmohamadi, A.M., Karimnejad, S., Mesoscopic Simulation of Forced Convective Heat Transfer of Carreau-Yasuda Fluid Flow over an Inclined Square: Temperature-dependent Viscosity, *Journal of Applied and Computational Mechanics*, 6, 2020, 307-319.

[18] Ashorynejad, H. R., Zarghami, A., Magnetohydrodynamics flow and heat transfer of Cu-water nanofluid through a partially porous wavy channel, *International Journal of Heat and Mass Transfer*, 119, 2018, 247-258.

[19] Sheikholeslami, M., Gorji-Bandpy, M., Domairry, G., Free convection of nanofluid filled enclosure using lattice Boltzmann method (LBM), *Applied Mathematics and Mechanics*, 34, 2013, 833–846.

[20] Sheikholeslami, M., Influence of magnetic field on Al2O3-H2O nanofluid forced convection heat transfer in a porous lid driven cavity with hot sphere obstacle by means of LBM, *Journal of Molecular Liquids*, 263, 2018, 472-488.

[21] Sajjadi, H., Salmanzadeh, M., Ahmadi, G., Jafari, S., Combination of Lattice Boltzmann Method and RANS Approach for Simulation of Turbulent Flows and Particle Transport and Deposition, *Particuology*, 30, 2017, 62-72.

[22] Benzi, R., Succi, S., Vergassola, M., The lattice Boltzmann equation: theory and applications, *Physics Reports*, 222, 1992, 145-197.

[23] Chen, S., Doolen, G., Lattice Boltzmann method for fluid flows, *Annual Review of Fluid Mechanics*, 30, 1998, 329–364.

[24] Lallemand, P., Luo, L., Theory of the lattice Boltzmann method: dispersion, dissipation, isotropy, Galilean invariance, and stability, *Physical Review E*, 61, 2000, 6546–6562.

[25] Ginzburg, I., Equilibrium-type and link-type lattice Boltzmann models for generic advection and anisotropic-dispersion equation, *Advances in Water Resources*, 28, 2005, 1171–1195.

[26] Chikatamarla, S., Ansumali, S., Karlin, I., Entropic lattice Boltzmann models for hydrodynamics in three dimensions, *Physical Review Letters*, 97, 2006, 010201.

[27] Luo, L., Liao, W., Chen, X., Peng, Y., Zhang, W., Numerics of the lattice Boltzmann method: effects of collision models on the lattice Boltzmann simulations, Physical Review E, 83 (5), 2011, 056710.

[28] Sajjadi, H., Amiri Delouei, A., Sheikholeslami, M., Atashafrooz, M., Succi, S., Simulation of three dimensional MHD natural convection using double MRT Lattice Boltzmann method, *Physica A*, 515, 2019, 474–496.

[29] Sajjadi, H., Delouei, A. A., Izadi, M., Mohebbi, R., Investigation of MHD natural convection in a porous media by double MRT lattice Boltzmann method utilizing MWCNT–Fe3O4/water hybrid nanofluid, *International Journal of Heat and Mass Transfer*, 132, 2019, 1087–1104.

[30] Sajjadi, H., Amiri Delouei, A., Atashafrooz, M., Sheikholeslami, M., Double MRT Lattice Boltzmann simulation of 3-D MHD natural convection in a cubic cavity with sinusoidal temperature distribution utilizing nanofluid, *International Journal of Heat and Mass Transfer*, 126, 2018, 489–503.

[31] Chang, T., Hsieh, Y., Kao, H., Numerical investigation of airflow pattern and particulate matter transport in naturally ventilated multi-room buildings, *Indoor Air*, 16, 2006, 136–52.

[32] Béghein, C., Jiang, Y. and Chen, Q., Using large eddy simulation to study particle motions in a room, *Indoor Air*, 15, 2005, 281–290.

[33] Zhang, Z., Chen, Q., Experimental measurements and numerical simulations of particle transport and distribution in ventilated rooms, *Atmospheric Environmental*, 40, 2006, 3396–408.

[34] Zhou, X., Dong, B., Chen, C., Li, W., A thermal LBM-LES model in body-fitted coordinates: Flow and heat transfer around a circular cylinder in a wide Reynolds number range, *International Journal of Heat and Fluid Flow*, 77, 2019, 113-121.

[35] Merlier, L., Jacob, J., Sagaut, P., Lattice-Boltzmann large-eddy simulation of pollutant dispersion in complex urban environment with dense gas

effect: Model evaluation and flow analysis, *Building and Environment*, 148, 2019, 634-652.

[36] Sajjadi, H., Salmanzadeh, M., Ahmadi, G., Jafari, S., Investigation of particle deposition and dispersion using Hybrid LES/RANS model based on Lattice Boltzmann method, *Scientia Iranica*, 25(6), 2018, 3173-3182.

[37] H. Sajjadi, M. Salmanzadeh, G. Ahmadi, S. Jafari, LES and RANS Model Based on LBM for Simulation of Indoor Airflow and Particle Dispersion and Deposition, *Building and Environment*, 102, 2016, 1-12.

[38] Amiri Delouei, A., Nazari, M., Kayhani, M. H., Succi, S., Non-Newtonian unconfined flow and heat transfer over a heated cylinder using the direct-forcing immersed boundary–thermal lattice Boltzmann method, *Physical Review E*, 89, 2014, 053312.

[39] Amiri Delouei, A., Nazari, M., Kayhani, M. H., Succi, S., Immersed Boundary – Thermal Lattice Boltzmann Methods for Non-Newtonian Flows over a Heated Cylinder: A Comparative Study, *Communications in Computational Physics*, 18, 2015, 489-515.

[40] Amiri Delouei, A., Nazari, M., Kayhani, M. H., Kang, S.K., Succi, S., Non-Newtonian Particulate Flow Simulation: A Direct-Forcing Immersed Boundary- Lattice Boltzmann Approach, *Physica A: Statistical Mechanics and its Applications*, 447, 2016, 1-20.

[41] Amiri Delouei, A., Nazari, M., Kayhani, M. H., Ahmadi, G., A Non-Newtonian Direct Numerical Study for Stationary and Moving Objects with Various Shapes: An Immersed Boundary -Lattice Boltzmann Approach, *Journal of Aerosol Science*, 93, 2016, 45–62.

[42] Tian, L., Ahmadi, G., Particle deposition in turbulent duct flows comparisons of different model predictions, *Journal of Aerosol Science*, 38, 2007, 377-397.

[43] Li, A., Ahmadi, G., Dispersion and deposition of spherical particles form point sources in a turbulent channel flow, *Aerosol Science and Technology*, 16, 1992, 209-226.

[44] Hardalupas, Y., Taylor, A., On the measurement of particle concentration near a stagnation point, *Experiments in Fluids*, 8, 1998, 113–118.

[45] Zhu, J., Rudoff, R., Bachalo, E., Bachalo, W.N., umber density and mass flux measurements using the phase Doppler particle analyzer in reacting and non-reacting swirling flows. *In: AIAA, Aerospace Sciences Meeting*, 1993.

[46] Salmanzadeh, M., Zahedi, Gh., Ahmadi, G., Marr, D.R., Glauser, M., Computational modeling of effects of thermal plume adjacent to the body on the indoor airflow and particle transport, *Journal of Aerosol Science*, 53, 2012, 29–39.

[47] Posner, J.D., Buchanan, C.R., Dunn-Rankin, D., Measurement and prediction of indoor air flow in a model room, *Energy Building*, 35, 2003, 515-526.

[48] Tian, Z.F., Tu, J.Y., Yeoh, G.H., Yuen, R.K.K., On the numerical study of contaminant particle concentration in indoor air flow, *Building and Environment*, 41, 2006, 1504–1514.

ORCID iD

H. Sajjadi https://orcid.org/0000-0002-0681-7682

G. Ahmadi https://orcid.org/0000-0001-5277-7960

A. Amiri Delouei https://orcid.org/0000-0001-7414-4195